Unusual Icosahedral Cluster Compounds: Open-Shell $Na_4A_6Tl_{13}$ (A = K, Rb, Cs) and the Metallic Zintl Phase $Na_3K_8Tl_{13}$ (How Does Chemistry Work in Solids?)

Zhen-Chao Dong and John D. Corbett*

Contribution from the Ames Laboratory—DOE[1] and Department of Chemistry, Iowa State University, Ames, Iowa 50011

Received December 28, 1994[⊗]

Abstract: The line phases in the title are obtained in high yields after fusion of the elements in stoichiometric proportions in Ta containers followed by slow cooling or annealing. The structures were established by single-crystal X-ray means [$Na_4A_6Tl_{13}$, A = K, Rb, Cs: $Im\bar{3}$, $Z = 2$, $a = 11.5075(7)$ Å, 11.6648(5) Å, 11.8332(4) Å, $R_w(F) = 2.9$, 4.9, 4.2%, respectively; $Na_3K_8Tl_{13}$: $R\bar{3}m$, $Z = 3$, $a = 11.0890(6)$ Å, $c = 23.154(2)$ Å, $R_w = 4.9\%$]. The structure of cubic $Na_4K_6Tl_{13}$ is practically identical with that reported for NaK_9Tl_{13}, a composition that cannot be achieved in this structure. The two structure types contain isolated, centered icosahedra of Tl_{13}^{10-} (T_h) and Tl_{13}^{11-} (D_{3d}) in *bcc* and *ccp* arrangements, respectively. All cations bridge between cluster faces or vertices, and their mixed sizes appear critical to the formation of the two structures containing these clusters, which do not occur in the binary systems. The phases exhibit Curie−Weiss (1.7, 1.9 μ_B) (cubic Rb, Cs) and temperature-independent ($\chi_M \sim 1.9 \times 10^{-3}$ emu/mol) (rhombohedral K) paramagnetism and poor metal-like resistivities ($\varrho_{293} = 310$, 625, 69 $\mu\Omega$·cm), respectively. The novel one-electron-deficient Tl_{13}^{10-} is a result of cation packing limitations, while Tl_{13}^{11-} fulfills (Wade's rule) predictions for a centered icosahedron. Centering of the clusters by thallium contributes markedly to the bonding in both. Theoretical calculations at the extended Hückel and relativistic Hückel (REX) levels for the clusters and at the LMTO (self-consistent band) level for $Na_4Rb_6Tl_{13}$ are all consistent with the experimental finding. Mixing of $6p_{1/2}$ and $6p_{3/2}$ levels in the clusters reduces relativistic separations substantially (to ~0.2 eV) relative to that in the free Tl atom. Electron localization within the clusters appears dominant.

Introduction

A variety of isolated thallium cluster anions have been synthesized and characterized in alkali metal−thallium systems.[2-6] The rich cluster chemistry is related to an approximate 1:1 atom: cluster charge ratio which allows (1) electronically for an appropriate number of electrons for the formation of deltahedral clusters with significant Tl−Tl bond strength and (2) structurally for a sufficient number of alkali metal cations embodied into the structure to efficiently separate the clusters. Such observations are also consistent with the strong relativistic effects for this heavy element.[7] Spin−orbit splitting stabilizes the Tl $(6p_{1/2})^2$ shell, causes an anomalously large electron affinity for the element, and makes the formal Tl^- state favorable. Parallel to electronic requirements, size factors also appear to play a crucial role in determining what cluster structures are formed. A number of novel thallium clusters not present in the binary systems have been successfully isolated by size tuning through mixing of alkali metals. These include the Tl_5^{7-} and Tl_9^{9-} clusters in $Na_2K_{21}Tl_{19}$[5] and the centered icosahedral polyanions in the title compounds.

The icosahedral unit of Tl, complete or defect, has been recurrently observed in our recent investigations. It functions either as a building block in the condensed binary cluster phases (e.g., A_4Tl_{13} (A = Rb, Cs) and $K_{23}Tl_{54}$[8]) or as a primary packing fragment in the ternary isolated cluster compounds. The latter are represented by (1) Tl_9^{9-}, a defect centered icosahedron missing four adjacent Tl atoms,[5] (2) $Tl_{10}M^{10-}$ (M = Ni, Pd, Pt), which can be viewed as defect M-centered icosahedra missing two adjoining vertices,[8] and (3) $Tl_{13}^{10-,11-}$ in the present examples and in the reported NaK_9Tl_{13},[9] a structure that we cannot reproduce at that composition. While icosahedral fragments are widely present in elemental boron, metallic borides,[10] gallides,[11] aluminides,[12] and indides,[13,14] isolated icosahedral clusters of other elements have only been reported for $[B_{12}H_{12}]^{2-}$,[15] its derivatives,[16] and $(Al\text{-}iBu)_{12}^{2-}$ [17] as well as some centered transition-metal clusters (e.g., $[Rh_{12}Sb(CO)_{27}]^{3-}$ [18] and $[Au_{13}Cl_2(PMe_2Ph)_{10}]^{3+}$ [19]). The icosahedron is the most stable geometry for 12-atom clusters because it maximizes the number of nearest neighbors on the spherical surface. Two other possible arrangements are the cuboctahedron and anticuboctahedron. Although isolated units of the latter

⊗ Abstract published in *Advance ACS Abstracts,* May 15, 1995.

(1) This research was supported by the Office of the Basic Energy Sciences, Materials Sciences Division, U.S. Department of Energy. Ames Laboratory is operated for the DOE by Iowa State University under Contract No. W-7405-Eng-82.

(2) Hansen, D. A.; Smith, J. F. *Acta Crystallogr.* **1967**, *22*, 836.
(3) Cordier, G.; Müller, V. *Z. Kristallogr.* **1992**, *198*, 281.
(4) Dong, Z.-C.; Corbett, J. D. *J. Am. Chem. Soc.* **1993**, *115*, 11299.
(5) Dong, Z.-C.; Corbett, J. D. *J. Am. Chem. Soc.* **1994**, *116*, 3429.
(6) Dong, Z.-C.; Corbett, J. D. *J. Cluster Sci.* **1995**, *6*, 187.
(7) Pyykkö, P.; Desclaux, J. P. *Acc. Chem. Res.* **1979**, *12*, 276.
(8) Dong, Z.-C.; Corbett, J. D. Unpublished research.
(9) Cordier, G.; Müller, V. *Z. Naturforsch.* **1994**, *49b*, 935.
(10) Matkovich, V. I., Ed. *Boron and Refractory Borides*; Springer-Verlag: Berlin, 1977.
(11) Belin, C.; Tillard-Charbonnel, M. *Prog. Solid State Chem.* **1993**, *22*, 59.
(12) Kreiner, G.; Franzen, H. F. *J. Alloys Compds.* **1994**, In press.
(13) Sevov, S. C.; Corbett, J. D. *Inorg. Chem.* **1992**, *31*, 1895.
(14) Sevov, S. C.; Corbett, J. D. *Inorg. Chem.* **1993**, *32*, 1612.
(15) Wunderlich, J. A.; Lipscomb, W. N. *J. Am. Chem. Soc.* **1960**, *82*, 4427.
(16) Beall, H., In *Boron Hydride Chemistry*; Muetterties, E. L., Ed.; Academic Press: New York, 1975; pp 302−347.
(17) Hiller, W.; Klinkhammer, K.-W.; Uhl, W.; Wagner, J. *Angew. Chem., Int. Ed. Engl.* **1991**, *30*, 179.
(18) Vidal, J. L.; Troup, J. M. *J. Organomet. Chem.* **1981**, *20*, 238.
(19) Briant, C. E.; Theobald, B. R. C.; White, J. W.; Bell, L. K.; Mingos, D. M. P. *J. Chem. Soc., Chem. Commun.* **1981**, 201.

0002-7863/95/1517-6447$09.00/0

Table 1. Selected Data Collection and Refinement Parameters for $Na_4A_6Tl_{13}$ (A = K, Rb, Cs) and $Na_3K_8Tl_{13}$

empirical formula	$Na_4K_6Tl_{13}$	$Na_4Rb_6Tl_{13}$	$Na_4Cs_6Tl_{13}$	$Na_3K_8Tl_{13}$
space group, Z	$Im\bar{3}$, 2	$Im\bar{3}$, 2	$Im\bar{3}$, 2	$R\bar{3}m$, 3
lattice parameters,[a] Å				
a	11.0575(7)	11.6648(5)	11.8332(4)	11.0890(6)
c				23.154(2)
no. of indep obsd refns ($I \geq 3\sigma(I)$), variables	196, 15	194, 15	211, 15	435, 29
μ, cm^{-1} (Mo Kα)	700.2	753.3	700.9	651.5
transmission range	0.75−1.62	0.54−1.32	0.56−1.27	0.67−1.24
residuals: R, R_w[b]	0.024, 0.029	0.045, 0.049	0.033, 0.042	0.038, 0.049

[a] Guinier data, λ = 1.540 562 Å, 23 °C. [b] $R = \sum||F_o| - |F_c||/\sum|F_o|$; $R_w = [\sum w(|F_o| - |F_c|)^2/\sum w(F_o)^2]^{1/2}$; $w = 1/\sigma^2$.

are rare in solids ($Rh_{13}(CO)_{24}H_5$ and $[Rh_{12}Pt(CO)_{24}]^{4-}$ [20]), they are more frequently found in condensed intermetallic phases.[21] However, except for Tl_{13}, the vertices in all of the polyatomic ions mentioned above are instead bonded to either ligands or like atoms in neighboring units.

In this article, we report further examples of how tuning with cation sizes can allow the isolation of remarkable cluster units not known in the binary alloys, the centered icosahedral polyanions of Tl_{13}^{10-} in $Na_4A_6Tl_{13}$ (A = K, Rb, Cs) (hereafter denoted as 4-6-13) and Tl_{13}^{11-} in $Na_3K_8Tl_{13}$ (hereafter denoted 3-8-13). These are striking polyanions not just because they are "naked" and isolated but also because both open-shell and closed-shell examples of basically the same cluster exist. The important effects of centering and cation size on bonding and stability are discussed. We also correlate the structures with the observed electrical and magnetic properties, for which those of the closed-shell $Na_3K_8Tl_{13}$ compound also provide further support for the concept of a "metallic Zintl phase" developed previously.[22,23] Efforts are also made to show, through these magnificent examples, how chemistry is involved in the synthesis, structure, bonding, and properties of the solids.

Experimental Section

Syntheses. All the syntheses were performed by reaction of the constituent elements. The surfaces of the Na chunks (99.9%, Alpha) and Tl metal bar (99.998%, Johnson-Mathey) were cleaned with a scapel before use, while the K (99.9%, Baker), Rb (99.9%, Alpha), and Cs (99.98%, Johnson-Mathey) were used as received sealed under Ar. The general reaction techniques in welded Nb or Ta tubing have been described elsewhere.[4,5] Because both reagents and products are very sensitive to air and moisture, all operations were carried out in N_2- or He-filled gloveboxes with typical humidity levels less than 0.1 ppm (vol).

No ternary phase diagrams are available for mixed alkali metal−thallium systems. Following both the binary phase diagrams of Thümmel and Klemm[24] and our experience, reaction mixtures were usually melted at ~500 °C and then slowly cooled to room temperature. The 4-6-13 phases were first discovered following reactions of compositions $Na_3A_4Tl_{11}$ (A = Rb, Cs) in welded Nb tubing that were homogenized at 400 °C for 1 week, and then slowly cooled to room temperature at 3 °C/h. Such reactions provided $Na_4A_6Tl_{13}$ in high yields (>90%) and A_4Tl_{13}[8] as minor products. The $Na_3K_8Tl_{13}$ phase was first discovered as the major product (>70%) (together with an unidentified and probably Na-richer ternary phase) after fusion of a $NaKTl_2$ composition in Ta tubing at 500 °C for 2 days, annealing at 250 °C for 30 days, and slow cooling (3 °C/h) to room temperature. Once the stoichiometries had been established by crystallography, *single phase* $Na_4A_6Tl_{13}$ (A = Rb, Cs) and $Na_3K_8Tl_{13}$ were obtained through stoichiometric syntheses from the constituent elements in Ta, fusion of the mixture at 500 °C for 1 week being followed by slow cooling (3 °C/h) to room temperature. Although fusion of $Na_4K_6Tl_{13}$ composition followed by slow cooling yielded only ~20% cubic $Na_4K_6Tl_{13}$ plus ~80% of the close-by $Na_3K_8Tl_{13}$, the yield of the target was raised to 95% (plus 3-8-13) by fast quenching of the melt from 500 °C followed by annealing at 300 °C for 1 week. We have been unable to achieve the synthesis of the reported NaK_9Tl_{13} phase;[9] instead, reactions at the designated composition carried out as above yield only K_8Tl_{11} (~40%) and $Na_3K_8Tl_{13}$ (~60%).

The size flexibilities of the two structures with respect to alkali-metal contents were also checked with the aid of powder diffraction data. Reactions starting with either $A_3A'_8Tl_{13}$ or $A_4A'_6Tl_{13}$ composition yielded (a) 4-6-13 but no 3-8-13 phases when A = Na and A′ = Rb or Cs and (b) A_8Tl_{11}-type phases as major products[6] (but no 3-8-13 or 4-6-13 products) when A = K or Rb and A′ = Rb or Cs. Sodium is evidently always required in the A positions while A′ = K distinguishes $A_3A'_8Tl_{13}$ from $A_4A'_6Tl_{13}$. Mixing of K, Rb, and Cs in the A′ positions was also tested, with answers of "no" for the 3-8-13 phase but "yes" for the 4-6-13 phases, for which the cubic lattice constants vary over the whole range for A′ = K−Cs from 11.51 (K) to 11.84 (Cs) Å.

X-ray powder patterns for samples mounted between pieces of cellophane were collected with the aid of an Enraf-Nonius Guinier camera, Cu Kα radition (λ = 1.540 562 Å), and NIST (NBS) silicon as an internal standard. Least-squares refinements of 38 to 64 lines indexed on the basis of the refined structural models resulted in the lattice constants given in Table 1. As is usually the case for compounds with isolated clusters, both $Na_4A_6Tl_{13}$ (A = K, Rb, Cs) and $Na_3K_8Tl_{13}$ appear to be line compounds (except of course when K, Rb, and Cs are mixed in the larger A′ site in the former); mixtures with different overall compositions gave the same cell parameters with deviations of less than 0.007 Å (10σ) for each. These materials are very reactive reducing agents, and traces of elemental Tl are sometimes seen as broad lines in the Guinier patterns whenever adventitious impurities, probably traces of H_2O, are encountered during exposure to the X-rays.

Property Measurements. The resistivities of pure phases were examined by the electrodeless "Q" meter method[6,25] for sieved samples of 93, 89, and 100 mg respectively of $Na_4Rb_6Tl_{13}$, $Na_4Cs_6Tl_{13}$, and $Na_3K_8Tl_{13}$. These had average grain sizes of ~200 μm and were diluted with chromatographic Al_2O_3. The "Q"-meter method is based on the change of the quality factor "Q" of an LC circuit caused by skin absorption in selectively sized grains when the sample is placed in the cavity of a coil. The resistivity values have been found to be correct within a factor of 3, while the temperature coefficients are more reliable. Measurements were made at 34 MHz over the range of 100−293 K. Magnetic susceptibility measurements on powdered $Na_4Rb_6Tl_{13}$ (23 mg), $Na_4Cs_6Tl_{13}$ (24 mg), and $Na_3K_8Tl_{13}$ (58 mg) at a field of 3 T were obtained over the range of 6−300 K with the aid of a Quantum Design MPMS SQUID magnetometer. Samples were held between two fused silica rods, which were in turn fixed inside a silica tube that was sealed at both ends under He. The raw data were corrected for the susceptibilities of the containers and the diamagnetism of the cores[26] as well as for the Larmor precession contribution of the delocalized valence electrons in the cluster orbitals.[5,13] The same samples for magnetic measurements were also used for ESR experiments, which were recorded with a Bruker ER-200D spectrometer (X-band) at 295 K.

Structure Determination. Black block-like crystals were picked up and sealed in thin-walled capillaries and then checked by Laue or

(20) Albano, V. G.; Ceriotti, A.; Chini, P.; Martinengo, S.; Anker, W. M. *J. Chem. Soc., Chem. Commun.* **1975**, 859.
(21) Chabot, B.; Cenzual, K.; Parthé, E. *Acta Crystallogr.* **1981**, *A37*, 6.
(22) Nesper, R. *Angew. Chem., Int. Ed. Engl.* **1991**, *30*, 789.
(23) Zhao, J.-T.; Corbett, J. D. *Inorg. Chem.* **1995**, in press.
(24) Thümmel, R.; Klemm, W. *Z. Anorg. Allg. Chem.* **1970**, *376*, 44.
(25) Shinar, J.; Dehner, B.; Beaudry, B. J.; Peterson, D. T. *Phys. Rev.* **1988**, *37B*, 2066.
(26) Selwood, P. W. *Magnetochemistry*, 2nd ed.; Interscience Publishers: New York, 1956; p 70.

Table 2. Positional Coordinates and Isotropic Thermal Parameters for $Na_4A_6Tl_{13}$ (A = K, Rb, Cs) and $Na_3K_8Tl_{13}$

atom	site symmetry	x	y	z	B_{eq} (Å^2)[a]
		$Na_4K_6Tl_{13}$			
Tl1	$m\bar{3}.$	0	0	0	0.8415(7)
Tl2	$m..$	0	0.24157(7)	0.14142(8)	1.50(5)
K	$mm2$	0.3284(7)	0	1/2	2.6(4)
Na	$.\bar{3}.$	1/4	1/4	1/4	1.378(3)
		$Na_4Rb_6Tl_{13}$			
Tl1	$m\bar{3}.$	0	0	0	1.141(1)
Tl2	$m..$	0	0.1406(1)	0.2378(1)	1.78(6)
Rb	$mm2$	0.1707(5)	0	1/2	2.7(2)
Na	$.\bar{3}.$	1/4	1/4	1/4	0.538(3)
		$Na_4Cs_6Tl_{13}$			
Tl1	$m\bar{3}.$	0	0	0	1.276(1)
Tl2	$m..$	0	0.1388(1)	0.2333(1)	1.92(5)
Cs	$mm2$	0.1701(2)	0	1/2	2.7(1)
Na	$.\bar{3}.$	1/4	1/4	1/4	0.478(3)
		$Na_3K_8Tl_{13}$			
Tl1	$\bar{3}m$	0	0	0	0.86(6)
Tl2	$.m$	0.10755(6)	−0.10755	0.10579(5)	1.33(2)
Tl3	$.m$	−0.16797(5)	0.16797	0.02376(4)	1.27(2)
K1	$3m$	0	0	0.2413(5)	2.1(3)
K2	$.m$	0.4656(4)	−0.4656	0.0824(3)	2.57(9)
Na	$.2/m$	1/2	0	1/2	0.7(6)

[a] $B_{eq} = (8\pi^2/3)\sum_i\sum_j U_{ij}a_i^*a_j^*\vec{a}_i\vec{a}_j$.

oscillation photography for their singularity. $Na_4K_6Tl_{13}$ data were collected on Rigaku AFC6R and the rest on an Enraf-Nonius CAD-4 diffractometer with graphite-monochromated Mo Kα radiation at 23 °C. Programmed indexing of 25 reflections from a random search over $13 \le 2\theta \le 30°$ yielded body-centered cubic cells for $Na_4A_6Tl_{13}$ and a rhombohedral cell (hexagonal setting) for $Na_3K_8Tl_{13}$. Two octants of data were measured in each case, with no absences imposed for $Na_4Rb_6Tl_{13}$, I-centering for $Na_4K_6Tl_{13}$ and $Na_4Cs_6Tl_{13}$, and R-centering for $Na_3K_8Tl_{13}$ after the last condition was confirmed for the first 500 reflections. Assignments of the space groups $Im\bar{3}$ for $Na_4A_6Tl_{13}$ and $R\bar{3}m$ for $Na_3K_8Tl_{13}$ were made on the basis of the systematic absences, statistical analyses of intensity distributions, and the subsequent successful refinements.

The structures were solved by direct methods.[27] Peak assignments were easily made in terms of both bond distances and peak heights. The serious absorption effects, with linear absorption coefficients around 700 cm^{-1}, were in each case corrected empirically according to, first, the average of the ψ-scan curves for five to eight strong reflections at different θ values and, subsequently, by DIFABS (as recommended)[28] after the isotropic refinement converged. Multiplicity refinements of Tl atoms (B's varying) with the alkali-metal atoms fixed indicated that the former sites are fully occupied with deviations of less than 3σ from unity. The inverse procedure gave the same answer for alkali-metal atoms in all cases except for Na, which gave seemingly over-occupied sites but with deviation of those from unity of less than 4σ. Fully occupied models were used in the final anisotropic refinements with secondary extinction corrections (at a $4-6\sigma$ significance level) included. All data reduction and structure refinements were performed using the TEXSAN package[29] on a VAX station. Some details of the data collections and refinements are listed in Table 1, the atomic positional and isotropic equivalent displacement parameters are in Table 2, and the important distances are given in Table 3. (No twinning or cells with different orientations were encountered for each of the cubic phases studied although such behavior is common for space group $Im\bar{3}$.) The generally more accurate Guinier-based lattice parameters were employed in all distance calculations. More details as well as anisotropic displacement parameters are contained in the supplementary material, and these as well as structure factor data are also available from J.D.C.

After the report of a NaK_9Tl_{13} composition[9] with substantially the same cubic structure as had been refined for $Na_4A_6Tl_{13}$ (A = Rb, Cs), we also refined the structure of the virtually identical $Na_4K_6Tl_{13}$, with the results summarized in Tables 1−3. Among the positional parameters, our coordinate of Tl2 deviates from that reported by 1.8σ while the other two differ by $<1\sigma$. The former affects Tl1−Tl2, the larger Tl2−Tl2, and the largest Tl2−K distances by 4.5 to 5σ, viz., 0.006, 0.007, and 0.014 Å, respectively; all others compare within 2σ. The isotropic equivalent thermal parameters obtained are generally smaller than before, especially for Tl1 and the fixed Na position. Lattice constants for different samples refined from Guinier data with the aid of Si as an internal standard are 11.5030(3) (for a Na-poor 3-7-13 composition), 11.5075(7), and 11.512(1) Å compared with 11.520(1) Å reported, evidently from diffractometer data. No great variation of a with loaded composition (Na-rich to Na-poor) could be detected, so a significant homogeneity region seems out of the question. The composition of NaK_9Tl_{13} came from the refinement of a 1:3 ratio of Na:K in the fixed site, without description of the process or the statistics but after a ψ-scan correction for absorption. Our refinement of the sodium site (with B varying) gave an occupancy of 82(5)% with B_{eq} = 0.4, in the opposite direction. Attempts to force a mixed Na + K occupancy with their sum constrained to unity and B_{eq} fixed at 2.6 Å^2 (that of the ordered K^+ site) allowed only 2.5% K, 50% of a single standard deviation.

In hindsight, refining light atoms at high symmetry sites (particularly those with inversion) presents particular problems. The influence of errors on temperature factors and, potentially, occupancies depends on the atomic number as well as the symmetry of the neighboring atoms, the tightness of the bonding sphere and, probably, the quality of the absorption correction. These effects appear to be clearly reflected in the thermal parameters for the Tl1 and the Na atoms in Table 2. B_{eq} values of centered Tl1 (or other) atoms are always smaller than those of the surface atoms, but the difference here is not large (~0.6 Å^2) thanks to the large atomic number of thallium. However, the influence on the light Na atom may be large, the B_{eq} value observed here decreasing as the other A′ cations became heavier. Of course, a multiplicity refinement in the latter situations can result in an over-occupied model for Na (but even so the deviations from unit occupancy were all within 4σ). Whether the model makes chemical sense or not seems the most important. The composition control demanded by a quantitative synthesis of a phase as judged by powder diffraction is most telling, probably as much as via many direct analyses (beyond crystallography). Unless clean single crystals can be picked out, direct analysis is of course no more informative than the composition loaded for such a reaction since no conventional fractionation is possible in these systems.

Results and Discussion

Syntheses and Composition. Even approximate phase diagrams are very useful guidelines for designing experiments, including starting compositions and heating profiles. Heating greatly facilitates the reaction, particularly when at least one of the components is a liquid. Slow cooling is usually employed in exploratory syntheses in order to obtain suitable crystals from the melts for X-ray characterization. The same procedure is also customary for a pure sample of a congruently melting compound once the composition is known from crystallography. On the other hand, rapid quenching from the melt followed by long annealing below the peritectic temperature is usually required in order to obtain a pure sample of an incongruently melting phase. Some special approaches (e.g., distillation) may also be needed in order to get pure phases of some problem peritectic compounds (e.g., CsTl).[8]

With the above information in mind, the observed product distributions from a considerable number of preparative reactions all indicate the following: (1) the presence of the small Na ion in a special site plus other larger alkali metals is decisive for the formation of the 4-6-13 and 3-8-13 cluster phases, no comparable phases being observed in the pure binary systems; (2) the proportion of Na in each of these icosahedral cluster phases is substantially invarient; (3) the melting of $Na_4A_6Tl_{13}$

(27) Sheldrick, G. M. SHELXS-86; Universität Göttingen, BRD, 1986.
(28) Walker, N.; Stuart, D. *Acta Crystallogr.* **1986**, *A39*, 158.
(29) TEXSAN, Version 6.0 package; Molecular Structure Corp.; The Woodlands, Texas, 1990.

Table 3. Bond Distances in $Na_4A_6Tl_{13}$ (A = K, Rb, Cs) and $Na_3K_8Tl_{13}$ (<4.5Å)

			$Na_4K_6Tl_{13}$	$Na_4Rb_5Tl_{13}$	$Na_4Cs_6Tl_{13}$	$Na_3K_8Tl_{13}$						
Tl1						Tl1				K1			
Tl1	Tl2	12×	3.222(1)	3.223(1)	3.213(1)	Tl1	Tl2	6×	3.2044(8)	K1	Tl2	3×	3.76(1)
Tl2						Tl1	Tl3	6×	3.273(1)	K1	Tl3	3×	3.548(5)[a]
Tl2	Tl1		3.222(1)	3.223(1)	3.213(1)	Tl2				K1	K2	3×	3.869(8)
Tl2	Tl2		3.255(3)	3.281(3)	3.285(2)	Tl2	Tl1		3.2044(8)	K1	K2	3×	4.77(1)
Tl2	Tl2	4×	3.421(2)	3.416(2)	3.402(1)	Tl2	Tl2	2×	3.578(2)	K1	Na	3×	3.638(6)
Tl2	A		3.671(5)	3.768(4)	3.882(2)	Tl2	Tl3		3.217(1)	K2			
Tl2	A	2×	3.923(4)	4.001(3)	4.087(2)	Tl2	Tl3	2×	3.4086(9)	K2	Tl2		3.811(8)[a]
Tl2	A		4.204(2)	4.264(2)	4.339(1)	Tl2	K1		3.76(1)	K2	Tl2	2×	3.813(2)
Tl2	Na	2×	3.1380(5)	3.1862(5)	3.2437(5)	Tl2	K2		3.811(8)	K2	Tl3	2×	3.810(5)
A						Tl2	K2	2×	3.813(2)	K2	Tl3	2×	3.819(5)
A	Tl2	2×	3.671(5)[a]	3.768(4)[a]	3.882(2)[a]	Tl2	Na	2×	3.1445(2)	K2	K1		3.869(8)
A	Tl2	4×	3.923(4)	4.001(3)	4.087(2)	Tl3				K2	K1		4.77(1)
A	Tl2	2×	4.204(2)	4.264(2)	4.339(1)	Tl3	Tl1		3.273(1)	K2	K2		4.04(1)
A	A		3.95(2)	3.98(1)	4.087(2)	Tl3	Tl2		3.217(1)	K2	K2	2×	4.40(1)
A	A	4×	4.264(4)	4.327(2)	4.392(1)	Tl3	Tl2	2×	3.4086(9)	K2	K2	2×	4.66(1)
A	Na	4×	4.168(2)	4.227(1)	4.2892(6)	Tl3	Tl3	2×	3.409(1)	K2	Na	2×	4.076(6)
Na						Nl3	K1		3.548(5)	Na			
Na	Tl2	6×	3.1380(4)	3.1862(5)	3.2437(5)	Tl3	K2	2×	3.810(5)	Na	Tl2	4×	3.1445(2)
Na	A	6×	4.168(2)	4.227(1)	4.2892(6)	Tl3	K2	2×	3.819(5)	Na	Tl3	2×	3.309(1)
						Tl3	Na		3.309(1)	Na	K1	2×	3.638(6)
										Na	K2	4×	4.076(6)

[a] Exo A−Tl bond distances.

is probably congruent for A = Rb and Cs, but incongruent for $Na_4K_6Tl_{13}$ since annealing is required for a high yield; (4) the rhombohedral $Na_3K_8Tl_{13}$ is probably congruently melting, but no equivalent compound exists for A′ = Rb or Cs; and (5) mixing of (K,Rb,Cs) within the larger A positions seems substantially nonexistent for $Na_3A_8Tl_{13}$, but it occurs in $Na_4A_6Tl_{13}$. The structural reasons for such product distributions are discussed below.

The structure refined here for $Na_4K_6Tl_{13}$, one of a series that also includes $Na_4Rb_6Tl_{13}$ and $Na_4Cs_6Tl_{13}$, is not only nominally isostructural with but also virtually identical to that recently reported for NaK_9Tl_{13}.[9] The following facts support the composition assigned herein: (1) The lattice and positional parameters and the resulting distances in the two are substantially identical, as described in the Experimental Section. (2) The 25% Na, 75% K occupation ascribed earlier to the small (Na) cation site produces impossibly short K−Tl distances of 3.14 Å (×6); for comparison, 3.49 Å is the least among many d(K−Tl) distances in the ordered $Na_2K_{21}Tl_{19}$ structure.[5] (3) The NaK_9Tl_{13} composition actually yields only K_8Tl_{11} and hexagonal $Na_3K_8Tl_{13}$ products at a detection limit of about 3%, while the reported "NaK_9Tl_{13}" was in fact isolated from a sodium-rich reaction composition.

Cluster Skeletons. The most remarkable common feature in all the title compounds is the presence of the isolated, naked, and centered icosahedral Tl clusters shown in Figure 1: (a) Tl_{13}^{10-} in $Na_4A_6Tl_{13}$ (A = K, Rb, Cs) and (b) Tl_{13}^{11-} in $Na_3K_8Tl_{13}$. These compounds contain the first examples of this size cluster among the triel family Tl, In, Ga, and Al. Neither has ideal icosahedral symmetry but rather T_h symmetry in Tl_{13}^{10-} and D_{3d} in Tl_{13}^{11-}. The size of Tl_{13}^{10-} undergoes only slight variations with the size of the large cation. The 12 equivalent center−surface distances decrease very slightly, 3.223(1)−3.213(1) Å, for K−Cs. The same is true for the distance between each surface Tl atom and its five equivalent neighbors which divide into two groups, a shorter member bisected by a 2-fold axis, between 3.257(2) and 3.285(2) Å, and four longer members at 3.423(1)−3.402(1) Å in the same order. In Tl_{13}^{11-}, there are two inequivalent surface atoms, and therefore the center−surface atom distances divide into two equal groups, 3.2044(8) Å to Tl2 and 3.273(1) Å to Tl3. The five connections around each surface atom are of three types, which still

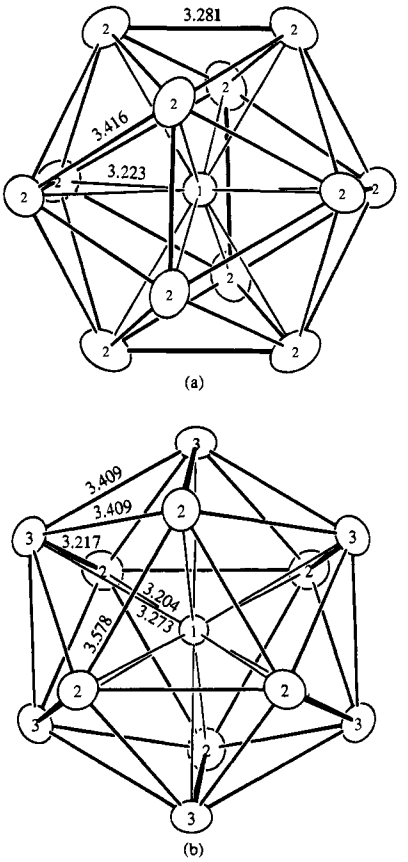

Figure 1. Centered icosahedral ions: (a) Tl_{13}^{10-} (T_h) in $Na_4Rb_6Tl_{13}$ where perpendicular 2-fold axes bisect the 3.281-Å edges; (b) Tl_{13}^{11-} (D_{3d}) in $Na_3K_8Tl_{13}$ with the 3-fold axis normal to the page (90% thermal ellipsoids).

effectively fall into a one short−four long combination (3.217−3.578 Å). One might expect a cluster size increase on the loss of one skeletal electron or with a change from K to Rb to Cs if judged simply from cation size. As a matter of fact, the opposite trend is observed. In the more reduced Tl_{13}^{11-} both the average center−surface and surface−surface distances, 3.239(1) and 3.404(1) Å, are actually slightly larger (~0.015 Å) than those in $Na_4K_6Tl_{13}$, and the distances in the latter series decrease

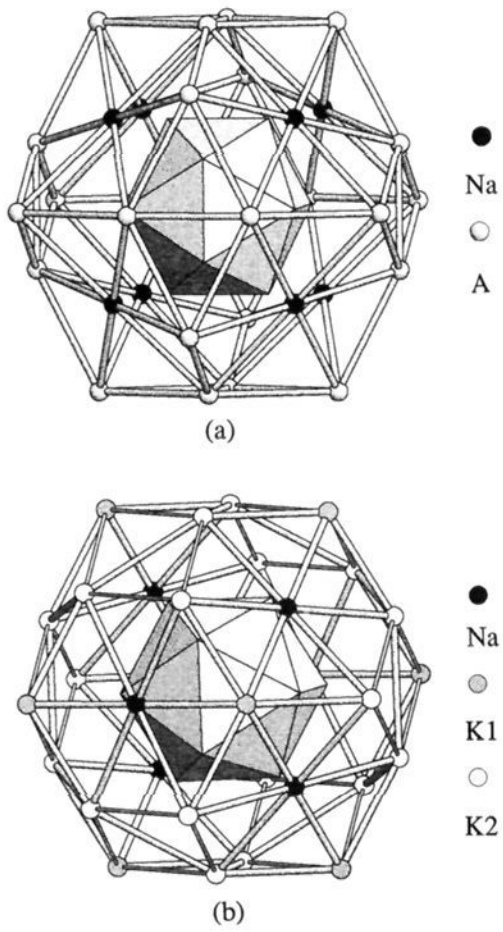

Figure 2. Cation arrangements around the icosahedral clusters: (a) truncated octahedra in $Na_4A_6Tl_{13}$ (A = K, Rb, Cs); (b) $Na_3K_8Tl_{13}$. The shaded polyhedra are the centered thallium icosahedra, which have the same orientations as in Figure 1.

further with Rb and Cs. Thus, shorter distances from increased electron localization on the cluster appear to parallel the decrease in electronegativity and polarizing power of the cations. Trends in other observed properties also follow from the same effects. As discussed below, the distortions of the icosahedral skeletons from the ideal $I_h \rightarrow T_h \rightarrow D_{3d}$ are basically driven by the cation packing requirements and are probably unrelated to the electronic factor even though the $I_h \rightarrow T_h$ portion coincides with the spirit of a Jahn−Teller distortion for an open-shell structure of Tl_{13}^{10-}.

Cation Distributions and Cluster Packings. The cation arrangements around icosahedral clusters and the cluster packings are depicted in Figures 2 and 3 for $Na_4A_6Tl_{13}$ and $Na_3K_8Tl_{13}$. The great importance of the apparent "solvation" of cluster anions by alkali-metal cations can hardly be overstated, as these effectively separate the clusters, create appropriate charge balance, and are crucial for the formation of a particular phase (as for the isoelectronic $In_{10}Zn^{8-}$ [30] vs $In_{10}Ni^{10-}$ [31]). As shown in Figure 3, cluster units form a *bcc* packing in cubic $Na_4A_6Tl_{13}$ but a pseudo-*ccp* rhombohedral stacking along the *c* direction in $Na_3K_8Tl_{13}$ ($c/a = 2.09$). The presence of sodium is essential for the formation of these icosahedral phases, but it is size factors for the other alkali metals that result in the different cluster packing patterns and stoichiometry (below). In each case, the thallium cluster unit is surrounded by 32 alkali metals functioning in two ways: 20 that cap each triangular face of the icosahedron and define a more or less distorted dodecahedral arrangement, and 12 that act as exo atoms at all thallium vertices (Figure 2). As is usually observed, the exo A−Tl interactions (A ≠ Na) are shorter than the face-capping A−Tl separations except for K2−Tl2 in $Na_3K_8Tl_{13}$ where they are similar (Table 3).

Polyhedral descriptions of the surrounding alkali metals are given below to help us to understand how clusters are interbridged or solvated by the alkali-metal atoms, but it should be kept in mind that such descriptions do not imply bonding interactions among the cation. In $Na_4A_6Tl_{13}$, the 24 A atoms form a slightly distorted truncated octahedron and the 8 Na atoms form a regular cube. While analogous geometries can still be identified in $Na_3K_8Tl_{13}$, they are strongly distorted because of structural and symmetry changes. (In order to indicate the encapsulation similarities, the long K1···K2 (4.77(1) Å) and K2···K2 (4.66(1) Å) contacts are drawn as thin rods in Figure 2b). The Na atoms, unlike the other alkali metals with dual bridging roles to adjoining clusters, have only face-capping functions and are located at the centers of puckered chair-like hexagons of the A metal in both structures (Figure 2). These puckered hexagons are shared by the neighboring clusters related by the *I*-centering (×8) or *R*-centering (×6) operations. Connections to six neighboring clusters related by cell translations are through shared cations, six truncated rhombuses (A_4 fragments) in $Na_4A_6Tl_{13}$ and six waist rhomboids formed by two K1 and two K2 atoms in an alternate sequence in $Na_3K_8Tl_{13}$ (K2−K2 = 4.04(1) Å, Figure 2).

Two questions arise naturally: (1) why are these isolated icosahedral phases only observed in ternary systems, and (2) why does the closed shell 3-8-13 structure not pertain when K is replaced by Rb or Cs rather than forming 4-6-13 with a loss of one of the eleven alkali metals needed to give a close-shell cluster? The answers are certainly related to cation size factors, specifically the size and shape of the coordination sphere around

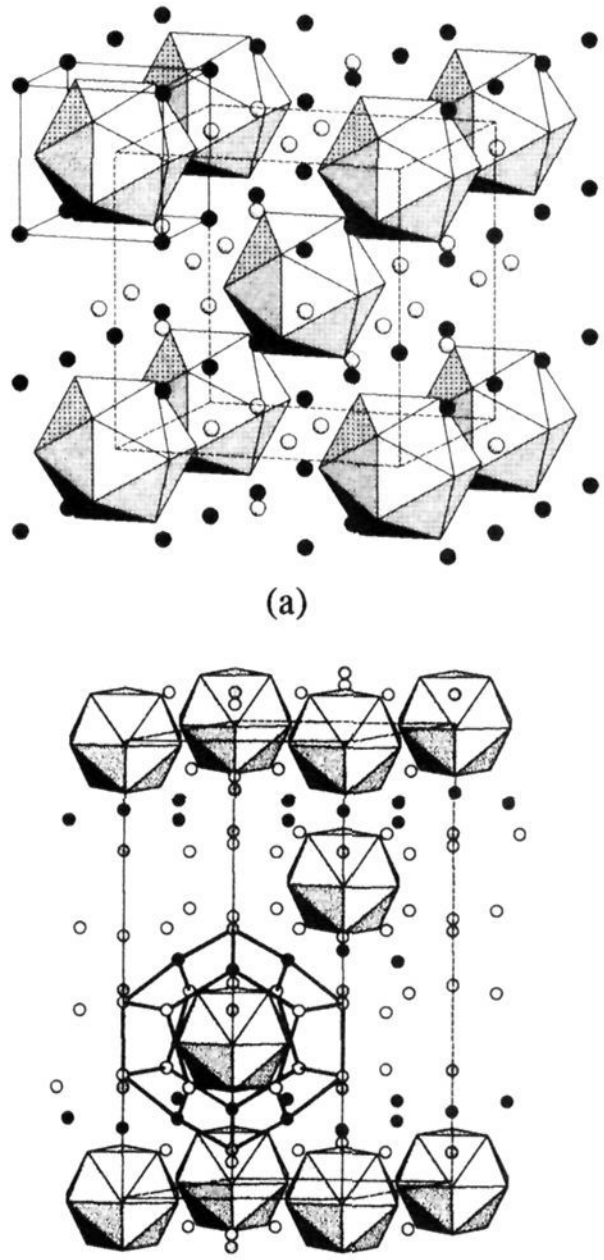

Figure 3. Cluster packing in a unit cell: (a) *bcc* packing in cubic $Na_4A_6Tl_{13}$ with the Na cube marked by thin lines; (b) pseudo-*ccp* rhombohedral stacking along the *c* direction with the distorted cation dodecahedron outlined. Symbols are the same as in Figure 2.

(30) Sevov, S. C.; Corbett, J. D. *Inorg. Chem.* **1993**, *32*, 1059.
(31) Sevov, S. C.; Corbett, J. D. *J. Am. Chem. Soc.* **1993**, *115*, 9089.

each individual alkali metal atom. The unique role of the Na atoms in the phase formation needs special attention. Like all Tl atoms in both structures, the Na atom is 12-coordinate in a distorted icosahedral environment, 6Tl + 6A. Its six Tl neighbors in two clusters form an elongated trigonal antiprism in $Na_4A_6Tl_{13}$ with six A atoms strongly squashed about the waist (i.e., the puckered chair-like hexagon). The same picture remains in $Na_3K_8Tl_{13}$ but it is distorted. The most important factor is the size of the sodium cavity. As seen in Table 3, the Na−Tl distances are ~3.2 Å, typical for that pair (3.24 Å in NaTl[32]). In other words, the packing is such that the Tl neighbors define a suitable hole for Na that is naturally too small for K, Rb, and Cs. (For comparison, the shortest A−Tl distances in A_8Tl_{11} are 3.57, 3.67, and 3.82 Å, respectively.[6]) The coordination differences between the 3-8-13 and 4-6-13 structure lie mostly in the positions of the larger alkali metals. In $Na_3K_8Tl_{13}$, there are six Tl neighbors for K1 (3Tl2 + 3Tl3) and seven for K2 (3Tl2 + 4Tl3). With the loss of one alkali-metal atom in $Na_4A_6Tl_{13}$, the number of Tl neighbors around the larger A atom increases to eight, as expected. Larger cavities at these positions are naturally reflected by the average A−Tl distances of 3.78, 3.92, 4.01, and 4.10 Å respectively in $Na_3K_8Tl_{13}$, $Na_4K_6Tl_{13}$, $Na_4Rb_6Tl_{13}$, and $Na_4Cs_6Tl_{13}$. Therefore, the formation of these icosahedral cluster phases is structurally related to the coexistence of both small and large cavities in structures that favor different sized cations and, furthermore, the small cavities can only be occupied by Na atoms. Of course, no parallels exist in the pure binary systems where other clusters such as Tl_{11}^{7-} are more stable. However, even these demand an extra cation in order to achieve good cluster−cation interactions, thus giving rise to novel metallic phases $(A^+)_8Tl_{11}^{7-}e^-$.[6]

Similar arguments regarding cavity sizes can be applied to rationalize the variation of the structural types from 3-8-13 to 4-6-13 and the product distributions in the syntheses. In $Na_3K_8Tl_{13}$, the Na−K distances are 3.638(6) Å to K1 (2×) and 4.076(6) Å to K2 (4×), but in $Na_4A_6Tl_{13}$, the Na−A distances are naturally much longer, from 4.168(2) Å for K to 4.2892(6) Å for Cs (6×). This means that if the K positions in $Na_3K_8Tl_{13}$ were occupied (fully or partially) by larger Rb or Cs atoms and the lattice also expanded correspondingly (~2%), the Na−Rb (or −Cs) distances would still be unreasonably short for a 3-8-13 model structure, with strong repulsions between these ionic pairs. The already-short 3.869 Å K1−K2 interactions in $Na_3K_8Tl_{13}$ would become particularly unfavorable if such substitution occurred. (Of course, the unanswerable question is the following: Is there not another packing that would do?) There is no way to insert one more alkali-metal atom into the 4-6-13 structure, because the largest hole in the structure is tetrahedral with a radius of 2.48 Å. This is chemically unacceptable because three of its neighbors are alkali metals and structurally impossible because it is too small to encapsulate even a lithium (Li−Tl distances in Li_5Tl_2 are ≥2.78 Å[33]). Fortunately, as discussed in the Bonding section, the loss of one cluster electron (and one alkali-metal cation) appears to have little influence on the overall stability of the icosahedral cluster when the relatively more open 4-6-13 structure forms. Analogous to the size flexibilities in A_8Tl_{11},[6] the A positions in $Na_4A_6Tl_{13}$ can also admix K, Rb, and Cs without changing the structural type (see Experimental Section−Syntheses).[34]

A strong "solvation" of cluster anions of this type by a large array of cations, as shown in Figure 2, is characteristic of all examples and is clearly related to their stability. Significantly shorter intercluster separations are presumably tantamount to instability. A recent theoretical prediction of a similar Al_{13} cluster in a metastable KAl_{13} would seem to be greatly lacking in that it utilized only a single K^+ cation per cluster in a simple cubic structure.[35] Further reduction of the cluster with the addition of more cations to the lattice would seem much more likely.

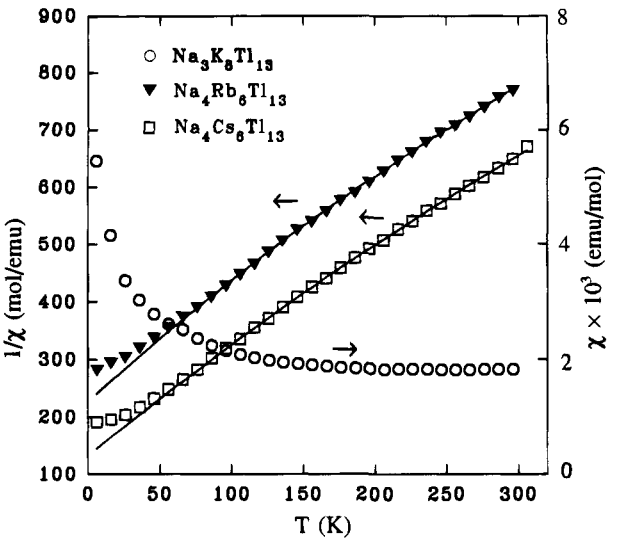

Figure 4. Temperature dependencies of molar susceptibilities at 3 T: $1/\chi-T$ plots for $Na_4A_6Tl_{13}$ (A = Rb, Cs) and $\chi-T$ plot for $Na_3K_8Tl_{13}$.

Properties and Bonding. Wade's rule predicts an optimal 26 ($2n$ + 2) skeletal electrons for an icosahedral cluster (Tl_{12}^{14-}).[36] The centered Tl_{13}^{11-} unit is also typical since the formal addition of a centered Tl^{3+} to this causes no change in the number of electrons or bonding states. The one-electron deficiency in the centered Tl_{13}^{10-} unit is directly reflected in the phase's magnetic and electrical properties. Magnetic measurements reveal a surprising, almost temperature-independent paramagnetism for $Na_3K_8Tl_{13}$ over 100−300 K with a susceptibility of ~1.9(1) × 10^{-3} emu/mol (corrected), while they yield a reasonable Curie−Weiss behavior for $Na_4A_6Tl_{13}$ (A = Rb, Cs) above ~50 K. The temperature dependencies of molar susceptibilities are illustrated in Figure 4 through a $\chi-T$ plot for the former and $1/\chi-T$ plots for the latter. Table 4 lists the Curie and Weiss constants and the background molar susceptibilities determined from a nonlinear fitting based on the function $\chi_M = C/(T-\theta) + \chi_0$. The u_{eff} values, 1.74(2) and 1.90(2) μ_B for $Na_4Rb_6Tl_{13}$ and $Na_4Cs_6Tl_{13}$, respectively, afford strong support for basically localized one-electron deficiency in these clusters. It is also interesting to see that antiferromagnetic interactions (if not ordering) begin to dominate near the $|\theta|$ temperatures. ESR spectroscopy for both shows a single spin with a g factor of ~2.01, while $Na_3K_8Tl_{13}$ is ESR silent, as expected for a paired system. Unfortunately, the hyperfine structure of 13 peaks expected for a single unpaired electron delocalized onto 12 equivalent surface Tl nuclei in the HOMO of Tl_{13}^{10-} (below) was not observed, presumably because the coupling is too weak and the side bands overlap strongly so that the fine structure is immersed in the central peak.

(32) Zintl, E.; Brauer, G. *Z. Phys. Chem.* **1933**, *20B*, 245.
(33) Stöhr, J.; Schäfer, H. *Z. Naturforsch.* **1979**, *34B*, 653.
(34) A data set was also collected on a cubic block-like crystal isolated from a reaction composition of $Na_4K_4Cs_2Tl_{13}$. The final refined composition was $Na_4K_{5.3(1)}Cs_{0.7}Tl_{13}$ with a = 11.519(7) Å, reflections/variables = 181/16, and R/R_w = 0.034/0.033. Similar lattice contractions were also observed for A′ = (K, Rb) or (Rb, Cs) according to the powder patterns. The preference for the smaller cation in the 6-fold position probably reflects the better Coulomb energy.
(35) Khanna, S. N.; Jena, P. *Chem. Phys. Lett.* **1994**, *219*, 479.
(36) Wade, K. *Adv. Inorg. Chem. Radiochem.* **1976**, *18*, 1.

Table 4. Resistivity and Magnetic Data and Intercluster Interactions for $Na_3K_8Tl_{13}$ and $Na_4A_6Tl_{13}$ (A = Rb, Cs)

	$Na_3K_8Tl_{13}$	$Na_4Rb_6Tl_{13}$	$Na_4Cs_6Tl_{13}$
ϱ_{293} ($\mu\Omega \cdot$ cm)	69	310	625
$\partial\varrho/\varrho\partial T$ (% K^{-1})	+0.28(3)	+0.29(2)	+0.24(3)
magnetic characteristics	Pauli paramagnetic	Curie–Weiss paramagnetic	Curie–Weiss paramagnetic
θ (K)		−92(6)	−62(4)
C		0.38(2)	0.45(2)
χ_0 (emu/mol)		$3.3(3) \times 10^{-4}$	$2.7(3) \times 10^{-4}$
μ_{eff} (μ_B)		1.74(2)	1.90(2)
ESR signal	silent	$g \sim 2.01$	$g \sim 2.01$
Tl_{13} center–center (Å)	10.0278(6) (6×)	10.1020(4) (8×)	10.2479(3) (8×)
	11.0890(7) (6×)	11.6648(5) (6×)	11.8332(4) (6×)
shortest intercluster Tl–Tl (Å)	5.172(1) (2×)	5.379(2) (4×)	5.524(2) (4×)

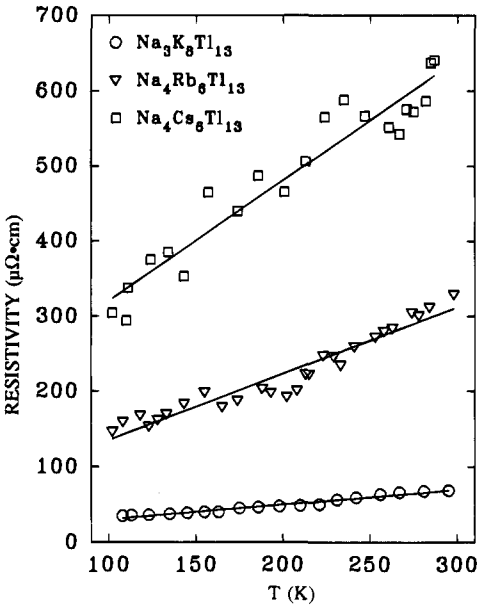

Figure 5. Resistivities versus temperature by the "Q" method.

Electron–nuclear double resonance techniques (ENDOR) might be helpful in this aspect.

Figure 5 shows the temperature dependencies of resistivities over 100–293 K for the same three compounds. (Numerical data are given in Table 4). Contrary to the semiconducting properties expected from the classical Zintl concept, positive temperature coefficients are observed for the resistivities of all three, so they are evidently metallic (or, perhaps, semimetallic). However, the classically paramagnetic $Na_4A_6Tl_{13}$ phases for A = Rb, Cs are very poor conductors as represented by their large resistivities (~300–600 $\mu\Omega \cdot$ cm), again indicating a basically localized picture of electrons with an electron hole within each cluster. The presence of such poor conduction for predicted closed-shell, diamagnetic cluster compounds of In and Tl has been a frequent observation, as will be described in the last section. On the other hand, the Pauli-like paramagnetism of the closed-shell $Na_3K_8Tl_{13}$ is consonant with a resistivity of only ~65 $\mu\Omega \cdot$ cm near room temperature, much higher than simple metals, say Al(ϱ_{298} = 2.65 $\mu\Omega \cdot$ cm), so that the valence electrons in $Na_3K_8Tl_{13}$ can still be viewed as largely localized, especially those that lie lower in the cluster bonding picture. Although conduction mechanisms for these compounds are not at all well understood, their sequence can be rationalized by the intercluster separations and the electronegativities of the alkali-metal atoms. As shown in Table 4, the intercluster distances increase from K to Rb to Cs as the polarizing (mixing) power and electronegativities of the cations decrease, logically leading to stronger localization and increased resistivities. (The changes in HOMO (LUMO) characteristics and bonds with the change in packing are probably also important.)

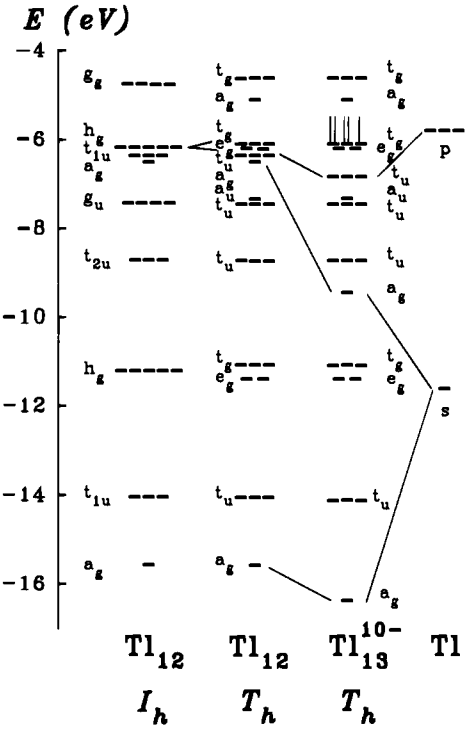

Figure 6. Extended-Hückel MO diagrams for hypothetical empty icosahedral Tl_{12} (I_h and T_h) and the observed centered icosahedral Tl_{13}^{10-} (T_h).

In order to better understand the structures and properties as well as their interrelations, electronic structure calculations were carried out on isolated icosahedral Tl_{13} clusters by standard EHMO methods.[37] For the sake of comparison and discussion, two hypothetical models, the regular icosahedral Tl_{12} (I_h, center–surface = 3.214 Å, surface–surface = 3.379 Å, the averages observed with Rb) and the observed polyhedron (T_h), were studied. Atomic parameters used for thallium were described in a previous paper.[4] The influence of distortion and centering on the bonding picture are clearly demonstrated in Figure 6. The change from regular I_h to the empty T_h generates little energy gain and hence does not seem a significant electronic factor. A clear, strong stabilization comes from the interstitialization. Centering makes the two radial a_g levels strongly bonding and the frontier tangential t_u orbital more bonding as well, originating with the added 6s and 6p orbitals, respectively. The calculations suggest the optimum electronic configuration has the first 25 valence MOs filled to present a Tl_{13}^{11-} polyanion with a HOMO–LUMO gap[38] of ~1.04 eV. However, with only ten cations in $Na_4A_6Tl_{13}$, the observed cluster is the open-shell anion Tl_{13}^{10-} with one unpaired electron (hole) in the HOMO t_g (or e_g) set. This electron is delocalized

(37) Hoffmann, R. *J. Chem. Phys.* **1963**, *39*, 1397.

among the twelve surface Tl atoms because orbital contributions from the central atom are not symmetry-allowed for t_g or e_g levels. Calculations were also performed on the observed Tl_{13}^{11-} (D_{3d}) in $Na_3K_8Tl_{13}$, which, of course, yielded a closed-shell structure. The MO diagram of $Na_3K_8Tl_{13}$ is not shown because it and the related bonding picture basically remain the same except that the t sets split into e and a levels in D_{3d} but by only 0.03 eV in the t_g HOMO.

Symmetry reduction of icosahedral clusters from T_h in $Na_4A_6Tl_{13}$ to D_{3d} in $Na_3K_8Tl_{13}$ is evidently not driven by electronic factors because there is no energetic or orbital power for a closed shell to do so. All distortions as well as the one-electron-deficient feature in $Na_4A_6Tl_{13}$ must be related to size factors or packing requirements of the particular cation (and anion) array in the extended structure. The electron-deficient character only slightly affects the Tl−Tl bond strengths; the average overlap population for each surface Tl−Tl bond remains almost unchanged from a Tl_{13}^{11-} unit (0.272) to Tl_{13}^{10-} (0.270), while the center−surface bond strength is not weakened at all because of symmetry. Therefore, the energetic loss from one electron must be small, and only the Coulomb contribution (vs $-\Delta H_F[A^+(g)]$) affects the overall stability of the networks. Judging by the overlap population analyses, a Tl_{13}^{9-} polyanion is also possible if cation size factors can be satisfied. Considering probable electron counts and these factors, efforts have been made to tune electron counts and to prepare (a) a closed-shell M-centered icosahedral $Tl_{12}M^{10-}$ (M = Ge, Sn, Pb) or (b) an empty Tl_{12}^{14-} cluster phase by mixing alkali and alkaline-earth metals, but so far all have failed. Obviously, the stability of the 3D structure is a dominate factor, and interstitialization of the cluster anions plays a great role. Further attempts are in progress.

In order to get some idea about the effects of the spin−orbit splitting on the bonding in these clusters, we have also applied a relativistically parameterized version of extended-Hückel theory called REX[39] to the problem. This method incorporates relativistic effects through atomic orbital basis sets with an $|lsjm>$ quantization (dual parameters for $p_{1/2}$ and $p_{3/2}$ of Tl) and through systematic parameterizations based on Desclaux' atomic relativistic Dirac−Fock and nonrelativistic Hartree−Fock calculations.[40,41] As long as spin−orbit coupling is introduced, double group notations[42] must be used to assign the MO symmetry. For the present purpose, what interests us most is the general bonding picture, not individual energy levels, to compare with experimental results. The resulting MO diagrams are not shown because REX calculations (as well as EHT results using appropriately averaged relativistic parameters) yielded basically the same bonding picture as the foregoing EHMO approach. The most apparent effect of spin−orbit splitting occurred for the t_g HOMO, which is no longer degenerate but splits into two spin−orbit components with a relativistic

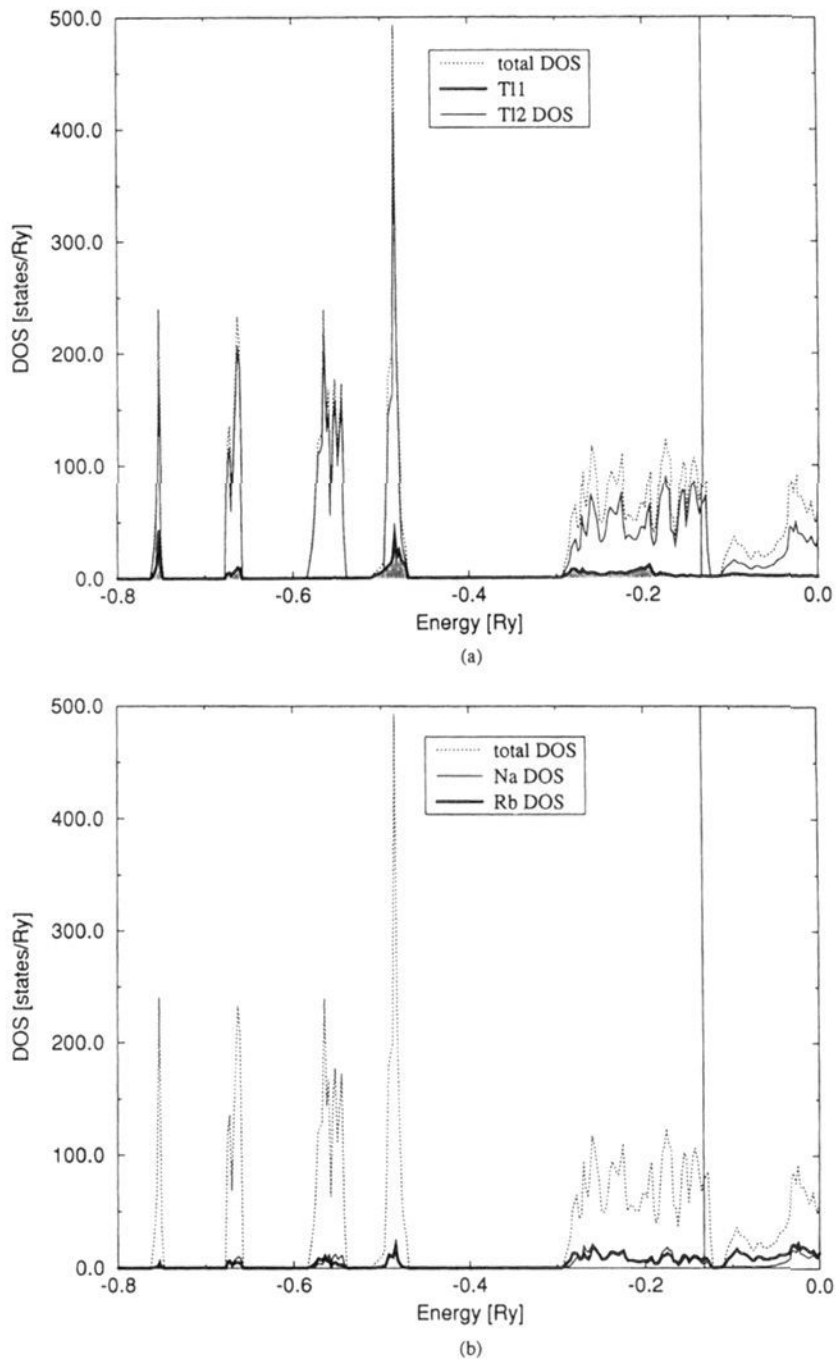

Figure 7. Densities of states (dashed) for $Na_4Rb_6Tl_{13}$ from LMTO calculations: (a) Tl contributions (solid lines); (b) Rb (heavy line) and Na (light line) contributions. Solid vertical lines mark the Fermi level.

separation of ~0.21 eV with respect to the EHT results.[41] (For comparison, the spin−orbit splitting of the frontier e_u level in the compressed D_{4h} Tl_6^{6-} octahedron[4] is ~0.20 eV.) The smaller relativistic separation found in clusters with respect to that in the elemental state (~0.95 eV[40]) results from the significant mixing of $6p_{1/2}$ and $6p_{3/2}$ shells when forming "molecules". One other feature is that the calculated total energy by REX is much lower (~60 eV/per cluster) in comparison with the EHT results, mostly because of the contraction and lower energy of the more nearly inert $6s^2$ pair, not from changes in the skeletal bonding. As a matter of fact, the bond strengths decrease when judged from net overlap populations; for instance, the net overlap population for a center−surface pair drops from 0.21 in EHT to 0.16 in REX, also a result of the more contracted p orbits in the latter.

Finally, the validity of the EHMO results is also supported by those from self-consistent (scalar-relativistic) linear-muffin-tin-orbit (LMTO) band calculations with the atomic sphere approximation (ASA)[43] on the full structure of $Na_4Rb_6Tl_{13}$. The DOS's shown in Figure 7 were calculated at 120 nonequivalent k-points with the total energy converging to better than 10^{-8}

(38) The t_g HOMO at −6.15 eV has a net overlap population of +0.13, and the a_g LUMO at −5.11 eV has a population of −0.31 according to the present calculation. However, the e_g level is within 0.03 eV to t_g, so their order might switch with different atomic parameters (e.g., EHT below). However, this has little effect on the overall bonding picture.

(39) Pyykkö, P. In *Methods in Computational Chemistry*; Wilson, S., Ed.; Plenum Press: New York, 1988; Vol. 2, p 137 and references therein.

(40) Desclaux, J. P. *At. Data Nucl. Tables* **1973**, *12*, 311. The atomic parameters for the relativistic calculations are as follows. EHT: $H_{ii}(6s) = -9.826$ eV, $\xi(6s) = 2.648$, $H_{ii}(6p) = -5.235$ eV, $\xi(6p) = 2.071$, REX: $H_{ii}(6s) = -12.223$ eV, $\xi(6s) = 3.036$, $H_{ii}(6p_{3/2}) = -4.804$ eV, $\xi(6p_{3/2}) = 2.063$, $H_{ii}(6p_{1/2}) = -5.751$ eV, $\xi(6p_{1/2}) = 2.357$. The orbital exponents are calculated via $\xi = (n + {}^1/_2)/r_{max}$, when n is the principal quantum number, and r_{max} is the radius of the maximum radial density. It is important to make comparisons on the basis of exactly comparable parameter sets.

(41) Pykkö, P.; Lohr, L. L. *Inorg. Chem.* **1981**, *20*, 1950.

(42) Altmann, S. L. *Rotations, Quaternions, and Double Groups*; Clarendon Press: Oxford, 1986.

(43) Andersen, O. K. *Phys. Rev.* **1975**, *B12*, 3060. Anderson, O. K. *Solid State Commun.* **1973**, *13*, 133. There are no empirical parameters with LMTO calculations. The only variable is the radius ratio of the elements involved, but with the constraint that the sum of the volumes of the elements should equal the volume of the unit cell. (This is why these radii are called Wigner−Seitz radii; Tl, 3.66662 au; Na, 3.59800 au; and Rb, 4.20000 au.)

Ry/cell. Figure 7a shows the thallium partial contributions and Figure 7b the alkali-metal projections. A very good correspondence is found between the molecular orbitals from EHMO and the bands from LMTO, with the energy levels of the latter roughly 5 eV higher because LMTO is a self-consistent method, and the bands' positions vary with the accumulated charges. The total energy is supposedly very close to the real total energy of the system. The finite DOS is present at E_F because of the (evidently localized) hole within the cluster, while E_F in this structure would lie in the gap for a closed-shell unit. Orbital contributions to the bands from the individual atom types are clearly seen in Figure 7. The poor metal-like conducting behavior of $Na_4Rb_6Tl_{13}$, as opposed to that of a more common paramagnetic insulator (with bound unpaired electrons), may be related to the fact that small contributions of the alkali metals to the bands aid the conduction process. We believe that the conductivity properties for all four title compounds may be associated with a semimetal-like band overlap model on the basis of the apparent cluster localization.

Conclusion

Solvation of $Tl_{13}^{11,10-}$ anions by Coulombic (and some covalent) interactions with the cations appears to establish a harmonious (balanced) "ionic packing" pattern. The specific roles of the alkali-metal ions about the cluster faces and vertices are to compensate anionic charge, often in two clusters simultaneously. The available alkali-metal positions are sometimes quite size-specific,[5] and sometimes not.[6] In the present examples, the Na position is very size-limited, typical for Na–Tl distances,[35] so that K or larger ions are too large to fit into this cavity, even partially.[6] Clearly, the presence of the small alkali-metal Na plays a decisive role in stabilizing these isolated icosahedral cluster phases because no analogues are found among purely binary phases. However, it appears that the size difference between K and Rb (or Cs), not the electronic requirements, is the major factor in determining which of the two icosahedral phases will form, and this fixes the cluster charge. A *ccp* packing is in general energetically more favorable than the *bcc* packing because the former has the higher space-filling efficiency, and a closed-shell Tl_{13}^{11-} salt is naturally more favorable energetically than that of an open-shell Tl_{13}^{10-}. The $Na_3K_8Tl_{13}$ structure appears to satisfy both requirements. On the other hand, when a hypothetical $Na_3K_8Tl_{13}$-type model is considered with Rb or Cs in place of K, the holes left between the icosahedral units are unfavorably small, and the comparatively less space-filling *bcc*-packed 4-6-13 structure forms instead to avoid strong Na–A repulsions. The more open *bcc* cluster packing also accounts for the greater size flexibility of the site A, tolerating K, Rb, and Cs as well as their mixtures in the $Na_4A_6Tl_{13}$-type structure.

The presence of a centering atom is probably decisive for formation of large clusters such as the icosahedron because it not only fills space more efficiently but also contributes significant central binding to the cluster. This is probably one of the reasons why efforts to make phases with an isolated Tl_{12}^{14-} ion have all failed, while the nonsphericity of large stable polyhedra (e.g., In_{16}^{13}) may account for the absence of centering there. The bonding between the interstitial and the peripheral atoms is delocalized in nature, and the impressive stabilization effect is best described within a molecular orbital framework. The overall phase stability comes from both the anionic substructure and the appropriate "solvation" of polyanions by cations. Such a picture is best portrayed starting with the Zintl–Klemm–Busmann concept,[44] that is, the transfer of electrons from the electropositive to the electronegative anions, as originally proposed, and the formation of a polyanionic substructure related to those of known isoelectronic elements. This has subsequently been modernized to include a great many valence compound networks and polyatomic ions that are not achieved by the elements.[45] The generalized term *Zintl ions* was later developed to describe a broader array of cluster systems, often with organic-based cations, with related but usually distinctive polyanions that exhibit nonclassical delocalized bonding and are unknown in neat intermetallic systems.[46,47] The skeletal electron counts in these can often be rationalized by electron counting rules (e.g., Wade's rules) derived from boranes and related species. Recently, the Zintl phase concept has been further applied to solid-state intermetallic compounds that have basically closed-shell bonding but still exhibit Pauli-paramagnetism and metallic conductivities, and hence may be usefully identified as *metallic Zintl phases*.[22,23] The new $Na_3K_8Tl_{13}$ fits into this last class perfectly. In fact, metallic conductivities, though often quite low, are observed for almost all alkali-metal In and Tl cluster compounds that have ideal closed-shell configurations for the latter.[4–6,13,14,30,31] These phases also present properties characteristic of Zintl phases:[44] brittleness, color, relatively fixed stoichiometry, and diamagnetism, the last changing to Pauli-paramagnetism only for clearly metallic phases. The general conduction behavior can perhaps be understood on the basis of a semimetal-like band overlap, the highest lying filled cluster orbitals (bands) slightly overlapping the neighboring cluster and cation states indirectly (or directly). The alkali-metal valence electrons are unlikely to be completely localized on the thallium cluster anions, rather a minor participation of alkali-metal orbitals with filled thallium states may allow appreciable time-average electron delocalization. But localization is dominant and the number of carriers is often very small. The point of all these conceptual extensions is to emphasize the spirit of the Zintl concept: *electron transfer (ionic part) and formation of a closed-shell anionic substructure (covalent part)*, and its utilization as a simple chemical guideline for designing experiments and understanding structure in broader ranges of systems.

Acknowledgment. We thank S. C. Sevov for the LMTO calculations and discussions, P. Pyykkö for advice on REX calculations, and J. Ostenson for the magnetic data.

Supplementary Material Available: Tables of crystallographic details and anisotropic displacement parameters (2 pages). This material is contained in many libraries on microfiche, immediately follows this article in the microfilm version of the journal, can be ordered from the ACS, and can be downloaded from the Internet; see any current masthead page for ordering information, and Internet access instructions.

JA944191F

(44) Zintl, E. *Angew. Chem.* **1939**, *52*, 1, Klemm, W.; Busmann, E. Z. *Anorg. Allg. Chem.* **1963**, *319*, 297.
(45) Schäfer, H. *Annu. Rev. Mater. Sci.* **1985**, *15*, 1.
(46) Corbett, J. D. *Chem. Rev.* **1985**, *85*, 383.
(47) Nesper, R. *Prog. Solid State Chem.* **1990**, *20*, 1.